ARTICLES

Scaling of the BMP activation gradient in *Xenopus* embryos

Danny Ben-Zvi[1], Ben-Zion Shilo[1], Abraham Fainsod[2] & Naama Barkai[1,3]

In groundbreaking experiments, Hans Spemann demonstrated that the dorsal part of the amphibian embryo can generate a well-proportioned tadpole, and that a small group of dorsal cells, the 'organizer', can induce a complete and well-proportioned twinned axis when transplanted into a host embryo. Key to organizer function is the localized secretion of inhibitors of bone morphogenetic protein (BMP), which defines a graded BMP activation profile. Although the central proteins involved in shaping this gradient are well characterized, their integrated function, and in particular how pattern scales with size, is not understood. Here we present evidence that in *Xenopus*, the BMP activity gradient is defined by a 'shuttling-based' mechanism, whereby the BMP ligands are translocated ventrally through their association with the BMP inhibitor Chordin. This shuttling, with feedback repression of the BMP ligand Admp, offers a quantitative explanation to Spemann's observations, and accounts naturally for the scaling of embryo pattern with its size.

Multicellular organisms develop with a remarkable consistency, maintaining a precise body plan in the face of genetic polymorphism or environmental fluctuations[1]. Yet, size and shape differ significantly even between closely related species. Developmental processes are thus shaped by seemingly opposing challenges: maintaining robustness at the species level, while allowing sufficient flexibility for evolutionary adaptation[2]. The interplay between robustness and evolutionary plasticity is poorly understood.

In Bilateria, early dorsoventral patterning relies on the graded distribution of BMP activity along the embryo. Two classical experiments performed by Hans Spemann (reviewed in ref. 3) demonstrated the dramatic plasticity of this patterning process in amphibians. First, dorsal halves of bisected embryos develop into well-proportioned tadpoles[4]. Second, cells taken from the embryonic dorsal blastopore lip and transplanted into the ventral side of a naive embryo induce a complete and well-proportioned secondary axis[5]. The region responsible for this induction property, 'Spemann's organizer', was identified later in other vertebrates, and its inductive capacity is attributed primarily to the secretion of BMP inhibitors[6]. However, the mechanism underlying the ability of dorsal-half embryos to grow into well-scaled tadpoles, and the ability to generate two complete and properly scaled tadpoles upon organizer transplantation, remained unknown. Experiments by Cooke further demonstrated the precision of scaling, and verified that compensation is not due to overgrowth of the remaining cells, but to their proportionate assignment to the different tissues[7].

Despite large differences in shape and size, the molecular network that generates the BMP gradient is remarkably conserved across evolution[8–11]. In flies and vertebrates, BMP ligands are initially expressed in broad domains, with the localized secretion of a conserved BMP inhibitor (Sog/Chordin, respectively[12,13]) providing the key organizing dorsoventral asymmetry[14,15] (Supplementary Fig. 1a–d). The inhibitors diffuse, undergo cleavage by a conserved protease (Tld/Xlr) and interact with a conserved modulator (Tsg/xTsg)[16–21]. Anti-dorsalizing morphogenic protein (Admp) is a BMP ligand found in many Bilateria but is missing in *Drosophila*. In contrast to other BMP ligands, it is expressed dorsally with BMP inhibitors, and is subject to autoregulatory transcriptional repression by the BMP pathway[22,23]. A role for Admp in providing scaling was recently suggested, following the observation that depletion of Admp abolishes patterning in dorsal-half embryos[24].

Theoretical analysis of the BMP gradient formation in the *Drosophila* embryo distinguished two qualitatively different patterning mechanisms[25–28] (Supplementary Fig. 1e, f). In the 'inhibition-based' mechanism, patterning is governed by the creation of an inhibition gradient over a uniform field of activators. In the 'shuttling-based' mechanism, patterning relies on the physical translocation of the activator to the midline, mediated by its binding to the inhibitor. Both mechanisms can generate a graded profile of BMP activation[26,29], but the finding that the shuttling mechanism generates a sharp and robust gradient led to the proposal that it is in use. This prediction was subsequently verified experimentally[26,30–32] (reviewed in refs 33 and 34). In this study, we show that shuttling is used also in the *Xenopus* embryo, and that, with the auto-repression of Admp, it ensures the scaling of the BMP activation profile with embryo size.

Shuttling is required for scaling

A key question is whether the conservation of network constituents implies the conservation of their integrated function, and if so, how an increased functional complexity can evolve. To examine whether shuttling plays a part in establishing the BMP activation gradient in *Xenopus*, we focused first on the ability of dorsal-half embryos to generate a well-proportioned embryo. This scaling property is difficult to explain by most models of morphogen gradients, and was proposed as evidence that patterning does not involve morphogens[7]. To assess the constraints imposed by this scaling property rigorously, we formulated a mathematical model that is based on the conserved core of this patterning network. The model includes two BMP ligands, Admp and Bmp (where Bmp stands for the three ligands BMP2/4/7), a BMP inhibitor (Chordin) and the protease Xlr (Fig. 1a). We allowed for the diffusion of all components, the binding of the BMP ligands to Chordin, and the degradation of Chordin by Xlr. We also considered the production of Chordin and Admp at the dorsal pole and the auto-repression of Admp by BMP signalling[24] (see Methods and Supplementary Information for equations and further details of the screen).

[1]Department of Molecular Genetics, Weizmann Institute of Science, Rehovot 76100, Israel. [2]Department of Cellular Biochemistry and Human Genetics, Faculty of Medicine, Hebrew University, Jerusalem 91120, Israel. [3]Department of Physics of Complex Systems, Weizmann Institute of Science, Rehovot 76100, Israel.

We screened systematically for parameters (rate constants and diffusion coefficients) for which the activation gradient is robust and scales with embryo size. To this end, we assigned each of the nine parameters three possible values, ranging over at least two orders of magnitude. The BMP activation gradient was solved numerically for all the networks defined in this nine-dimensional cube. Of the 26,000 networks examined, approximately 1,100 displayed a proper polarity, but only 21 were also capable of scaling in a dorsal-half embryo. An example for a gradient that did not scale is shown in Fig. 1b, d whereas a scaled gradient is shown in Fig. 1c, e. Examining the solutions, we noted that the respective gradients were established by distinct mechanisms. In the network that did not scale, the overall level of the ligands remained approximately uniform, and the activation gradient reflected the gradient of the inhibitor Chordin. In contrast, in the network that did scale, the ligands were physically concentrated at the ventral pole. The activation gradient was thus generated by the shuttling of the ligands to the ventral pole.

To examine more generally whether shuttling is required for scaling, we defined a rigorous measure that quantified the extent of shuttling, namely the translocation of the total ligand to the ventral pole, in each of the networks tested (Methods and Supplementary Information). Shuttling was observed in all networks that were capable of robust scaling (Fig. 1f). Moreover, the parameters of the consistent networks obeyed the molecular requirement for shuttling, as described previously in *Drosophila*[26]. First, the binding of Chordin to the BMP ligands largely facilitated the diffusion of the BMP ligands (Fig. 1g–j). Second, Chordin was degraded primarily when complexed with BMP ligands (Fig. 1g, h). Additionally, we found that scaling requires that Chordin binds to Bmp with a significantly higher affinity than to Admp (Fig. 1i, j).

Mechanism by which scaling is achieved

Our numerical analysis confirmed that the known patterning network can support the scaling of pattern with size, and suggested that shuttling plays an important part in providing this ability. To

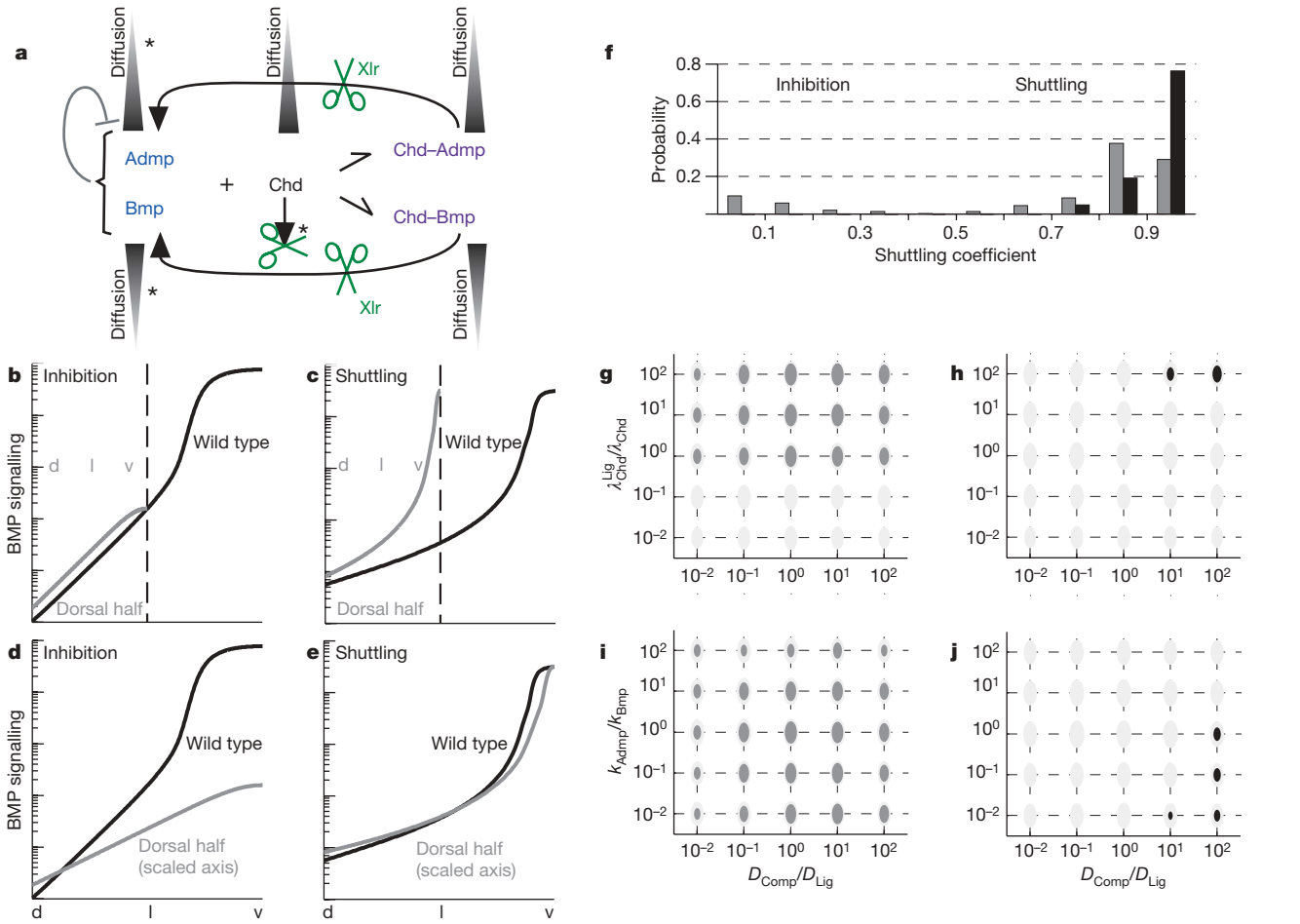

Figure 1 | Numerical evidence for shuttling. a, Model used in the screen. See Methods and Supplementary Information for equations and parameters. **b**, **d**, Activation profiles defined by the inhibition-based model. The model assumes that all components diffuse at the same rate. The model was solved numerically for the whole embryos (black) and the dorsal-half embryos (grey). The unscaled profile, measured in absolute length, is shown in **b** whereas the scaled profile measured in relative lengths, scaled by the size of the field, is shown in **d**. d, l, v, dorsal, lateral and ventral regions of the embryo, respectively. **c**, **e**, Activation profiles defined by the shuttling-based model. The model assumes free-ligand diffusion is much smaller than that of Chordin and the complex. Chordin is degraded primarily when complexed with a BMP ligand (parameters marked with * in Fig. 1a are small). The unscaled profile is shown in **c** whereas the scaled profile is shown in **e**. **f**, Consistent networks establish pattern by shuttling. Distribution of the shuttling coefficient S_h in consistent networks (black) and in all the networks that establish a dorsoventral gradient (grey). $S_h \approx 1$ indicates a shuttling mechanism, whereas $S_h \approx 0$ an inhibition mechanism. **g**, **h**, Relative diffusion and degradation in networks that establish dorsoventral polarity. The *x* axis displays the ratio between diffusion coefficients of the inhibitor-bound and free BMP ligand (D_{Comp}/D_{Lig}). The *y* axis displays the ratio between degradation of BMP-bound and free inhibitor $\left(\lambda^{Lig}_{Chd}/\lambda_{Chd}\right)$. Networks that were sampled in the screen are in light grey. Because this plot is a projection from a nine-dimensional space, each point symbolizes many networks where the respective ratios were held fixed, but parameters were changed systematically. **g**, Grey circles correspond to networks establishing proper dorsoventral polarity. **h**, Black circles correspond to networks establishing proper dorsoventral polarity, support scaling and robustness. **i**, **j**, Affinity of Chordin to Admp versus Bmp. Same as **g**–**h** with the *y* axis denoting the ratio between of binding rates of Chordin to Admp and Bmp (k_{Admp}/k_{Bmp}).

understand better how scaling is achieved we analysed the shuttling mechanism in more detail (Supplementary Information). As we have shown previously[26], shuttling of a single ligand leads to an activation profile that decays as a power law:

$$S(x) \approx \frac{S_0^{\mathrm{Lig}}}{x^2}; \quad S_0^{\mathrm{Lig}} = \frac{2D_{\mathrm{Chd}}}{k_{\mathrm{Lig}}} \qquad (1)$$

where D_{Chd} is the Chordin diffusion coefficient and k_{Lig} is the binding rate of the BMP ligand to Chordin. This profile is valid in most places, ($x > \varepsilon$ with $\varepsilon \propto 1/[\mathrm{BMP}]_{\mathrm{tot}} \to 0$). It is robust to changes in the levels of network components but does not scale with embryo size; indeed, embryo size does not appear in equation (1), and thus does not influence the shape of the gradient. Similarly, solving the model numerically under conditions of secondary-axis induction, we find that two axes ensue, but these two axes decay at the same rate as the original axis and do not scale to half-embryo size (Fig. 2a–c).

Thus, shuttling of a single ligand is not sufficient for scaling. We extended the model to account for the additional ligand Admp, and its feedback-mediated repression. This model can also be solved analytically (Box 1), predicting the activation profile:

$$S(x) \approx \frac{T_{\mathrm{Admp}}}{(x/L)^2} \qquad (2)$$

where T_{Admp} denotes the BMP concentration threshold at which *admp* is repressed. Again, this profile is valid in most positions x. This activation profile has two important consequences. First, the shape of the profile depends only on T_{Admp} and is independent of the other parameters in the system. Accordingly, the profile is robust to fluctuations in most parameters (Fig. 2g). Experimental support for this robustness is provided by the fact that depletion of *bmp2*, *bmp4* or *bmp7*, as well as the partial depletion of Chordin using antisense morpholino directed against one of the *chordin* pseudo alleles, display only a minor phenotype[35,36].

A second notable feature of the activation profile equation (2) is the explicit scaling of position (x) with embryo length (L). In fact, the activation profile is a function of the ratio x/L, implying the scaling of pattern with size. For example, a gene that is normally induced at 50% embryo length ($x/L = ½$) will be expressed at 50% embryo length irrespective of embryo size, and in particular will be found in the middle of a dorsal-half embryo (Fig. 2h). Moreover, solving the model under conditions of secondary-axis induction, with the addition of ventral source of secreted inhibitor, we find the two axes are now properly scaled (Fig. 2i). Indeed, this scaling of the twinned embryo can be readily explained by equation (2): when two sources of inhibitor are present at opposite poles, the symmetry positions the new ventral side at the mid-point ($x = L/2$), and each gradient is now defined separately with respect to this point. The resulting twinned gradients will thus be given by equation (2), with an effective embryo length of $L/2$.

Experimental evidence for shuttling

The shuttling mechanism predicts three molecular features that are required for this mechanism. First, the binding of Chordin to Bmp is predicted to be of higher affinity than its binding to Admp, an assessment that is supported by the relatively high concentrations of Chordin required for Admp inhibition[22]. Second, cleavage of Chordin is predicted to occur primarily when in complex with a BMP ligand. Chordin is in fact degraded by Xlr also in the absence of BMP, at least *in vitro*[21]. We propose that the formation of an xTsg–BMP complex, which facilitates both the binding of BMPs to Chordin and the degradation of the tertiary complex Chordin–xTsg–BMP, accounts for this assumption.

The third, key prediction of our model is the shuttling of Bmp and Admp by Chordin away from their domain of production. Shuttling requires that the BMP ligands diffuse primarily when bound to Chordin. An attenuated (effective) diffusion of free BMP can be achieved by various mechanisms, including binding to immobilized receptors or elements of the extracellular matrix[37], rapid degradation of receptor-bound ligand[38] or excessively high abundance of Chordin[39] (Supplementary Information). Although the diffusion of the BMPs was not assayed directly, it was shown that in animal caps, which do not express Chordin, BMP4 functions as short-range ligand[40].

To examine the predicted shuttling, we injected messenger RNA coding for Myc-tagged BMP4 into the dorsal part of early embryos, and followed its distribution by direct immunostaining at a later stage. The original injection site was marked by the co-injection of mRNA encoding cytoplasmic green fluorescent protein (GFP). In a parallel experiment, we injected the Myc-tagged *bmp4* mRNA with *chordin* morpholino, thus depleting Chordin, the presumed shuttling molecule. As predicted, we found that BMP4–Myc is shuttled to the

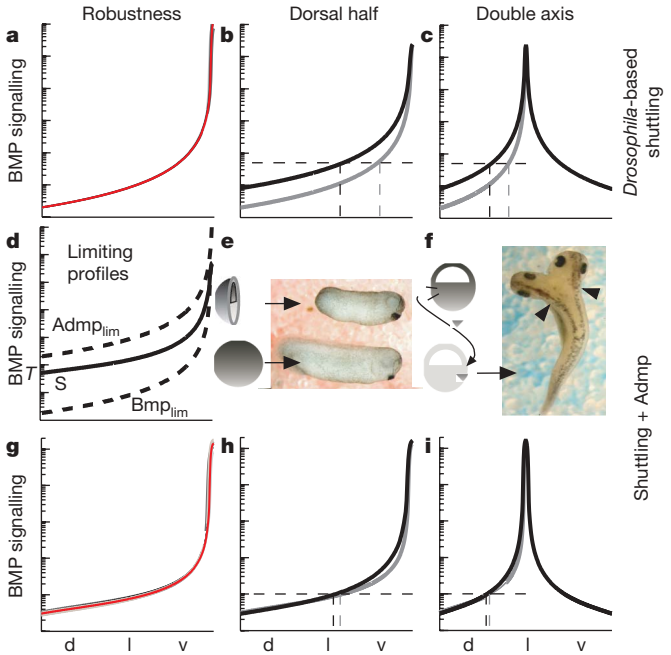

Figure 2 | Shuttling model supports size compensation and secondary-axis induction. **a–c**, 'Core' shuttling model. The model consists of a single BMP ligand that is not subject to auto-repression. **a**, Robustness to twofold decrease (dashed line) or increase (full line) in the production rate of BMP (light grey), Chordin (dark grey) and the protease (black). Unperturbed system profile in red. All profiles are virtually overlapping. **b**, BMP activation profile in wild type (grey) and dorsal-half embryo (black). **c**, BMP activation profile in wild-type embryo (grey) and in embryos with an added ventral source of inhibitor (black). The x axes in **b** and **c** are scaled to embryo length. **d–i**, *Xenopus*-based shuttling. The 'core' shuttling model was extended to include also Admp and its auto-repression by the BMP pathway (Box 1). This model now includes two ligands (Bmp and Admp), both of which can bind Chordin, albeit with a different affinity. d, l, v, dorsal, lateral and ventral, respectively. **d**, Activation profile of *Xenopus*-based shuttling. Each BMP ligand can be associated with a 'limiting profile', based on its predicted behaviour by the *core* shuttling mechanism, denoted by $\mathrm{Admp}_{\mathrm{lim}}$ and $\mathrm{Bmp}_{\mathrm{lim}}$ (dashed lines). The actual signalling profile, S (black), is a weighted average of the two limiting profiles, and can obtain any intermediate value, depending on the relative levels of Admp and Bmp (Box 1). Because Admp is subject to auto-repression, its level at the dorsal-most region is set to the repression threshold, T. This is possible only when $\mathrm{Admp}_{\mathrm{lim}} > \mathrm{Bmp}_{\mathrm{lim}}$, implying a tighter binding of Chordin to Bmp than to Admp. **e**, Scaling of dorsal-half embryos. A dorsal-half embryo in tadpole stage compared with a sibling wild-type embryo. **f**, Double axis. Dorsal view of an embryo with a double axis. Arrowheads point to the two axes. **g–i**, Robustness and scaling. **g**, The extended shuttling model maintains its robustness for ligand distribution. **h**, In addition, it supports the precise scaling of pattern with size. **i**, The extended model ensures precise axis duplication upon ventral transplantation of an organizer. Medium grey in **g** denotes double or half Admp production rate (full/dashed). Other line colours in **g–i** are as in **a–c**. The x axis in **h–i** is scaled to embryo length. See Supplementary Information for the parameters used.

Box 1 | 'Shuttling mechanism' in the *Xenopus* network: model formation

Our model is based on the shuttling mechanism[26]. The 'core' shuttling model previously described[26] considers a single BMP ligand whose total levels are fixed in time. Here, we extend this model to include two BMP ligands: Admp and Bmp, and to account for the auto-repression of *admp* by the BMP pathway activation. This model is obtained as a limiting case of the more general set of equations used in our numerical screen (equation (3)), by assuming that the free ligands do not diffuse ($D_{Lig} = 0$), and that the free inhibitor is not degraded ($\lambda_{Chd} = 0$). We are interested in the activation profile, $S(x) = [Bmp](x) + [Admp](x)$, as measured at steady state. This can be derived by solving the following set of equations:

$$0 = D_{Chd}\nabla^2[Chd] - k_{Admp}[Chd][Admp] - k_{Bmp}[Chd][Bmp]$$

$$0 = -k_{Admp}[Chd][Admp] + \lambda_{Chd}^{Admp}[XIr][ChdAdmp]$$

$$0 = -k_{Bmp}[Chd][Bmp] + \lambda_{Chd}^{Bmp}[XIr][ChdBmp] \quad (4)$$

$$0 = D_{Comp}\nabla^2[ChdAdmp] + k_{Admp}[Chd][Admp] - \lambda_{Chd}^{Admp}[XIr][ChdAdmp]$$

$$0 = D_{Comp}\nabla^2[ChdBmp] + k_{Bmp}[Chd][Bmp] - \lambda_{Chd}^{Bmp}[XIr][ChdBmp]$$

We consider one-dimensional geometry (Supplementary Information), with the dorsal-most region at $x = L$ and the ventral-most at $x = 0$. We assume that all fluxes of the diffusing quantities ([*Chd*], [*ChdAdmp*] and [*ChdBmp*]) vanish at $x = 0$. At ($x = L$), [*Chd*] is produced with a constant flux $\left(D_{Chd}\frac{d[Chd]}{dx}_{x=L} = \eta_{Chd}\right)$, whereas the fluxes of the complexes are zero.

Defining $S_0^{Lig} \equiv 2D_{Chd}/k_{Lig}$, ligand being Admp or Bmp, the solution to equation (4) is given by (see Supplementary Information, section 3):

$$Admp(x) = (1-\delta)\frac{S_0^{Admp}}{x^2+\varepsilon^2}; Bmp(x) = \delta\frac{S_0^{Bmp}}{x^2+\varepsilon^2} \quad (5)$$

where $0 < \delta < 1$ is a constant that depends on the relative levels of total Admp versus total Bmp

$$\delta = \frac{k_{Bmp}Bmp^{tot}}{k_{Bmp}Bmp^{tot} + k_{Admp}Admp^{tot}} \quad (6)$$

and ε is an integration coefficient whose level is inversely proportional to the average total level of the two BMP ligands in the system. The robust scaling solution is obtained when this level is sufficiently large, so that $\varepsilon \ll L$. In this case, the signalling level in most places in the embryo is given by:

$$S(x) \approx \frac{S_0}{x^2}; S_0 = (1-\delta)S_0^{Admp} + \delta S_0^{Bmp} \quad (7)$$

As noted above, δ, and accordingly S_0, depends on the relative level of Admp versus Bmp. Thus, a range of solutions is possible. In fact, depending on δ, the solutions can lie anywhere between the limiting solution corresponding to the case where only Bmp is present ($\delta = 1$) to the limiting solution obtained when only Admp is present ($\delta = 0$). This provides the system with the flexibility to define the precise solution by self-regulating the levels of Admp and Bmp and thus of δ. The scaled solution is obtained when the following three conditions are satisfied. First, Chordin binds Bmp with a higher affinity than Admp ($k_{Bmp} > k_{Admp}$) as we observed numerically (Fig. 1i, j). The lower affinity of Chordin to Admp allows for the accumulation of free Admp; consequently, the limiting profile corresponding to Bmp only is lower than the profile corresponding to Admp only (Fig. 2d). Second, Bmp levels are relatively fixed in time (its production and degradation are balanced), but Admp continues to accumulate as long as it is produced (exhibits a slow degradation). Third, Admp is repressed by BMP signalling, and the repression threshold T_{Admp} allows for its full repression throughout the embryo at some intermediate profile $0 < \delta < 1$. Steady state will be achieved when Admp has accumulated to just the right level to repress its own production everywhere, and in particular at the dorsal-most pole, where signalling level is lowest. Note that we assume that the level of free ligand is sufficient for signalling in the presence of high levels of Chordin. Thus, steady state is obtained when $S(x = L) = T_{Admp}$. Substituting this condition into the signalling profile, equation (7), we obtain the scaled solution (equation (2) in main text):

$$S(x) \approx \frac{T_{Admp}}{(x/L)^2} \quad (8)$$

which is valid for most positions of the embryo that satisfy $x > \varepsilon$. In the Supplementary Information we show that this same activation profile is indeed obtained as a numerical solution of the full dynamics, and can be realized within an extended model that includes additional known components of the patterning network.

ventral pole in embryos that expressed Chordin (Fig. 3b–e), but remains tightly localized to the dorsal pole in the embryos that were depleted of Chordin (Fig. 3f–i). This experiment thus provides direct evidence for the shuttling of BMP4 away from its site of production, and verifies that Chordin is required for this shuttling.

To verify further that shuttling is used during the patterning process itself, we examined the expression domains of ventral genes during secondary-axis induction. Ventral injection of *siamois* (*sia*)

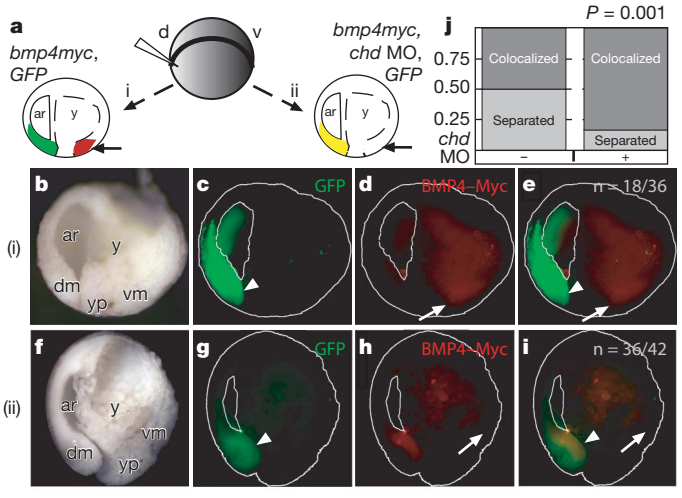

Figure 3 | Direct visualization of BMP4 shuttling by Chordin. **a**, Experimental design. Embryos at the two-cell stage were co-injected on the dorsal side with *bmp4myc* (400 pg) and *GFP* (260 pg) mRNAs, with or without *chordin* morpholino (250 μM). Embryos were grown to stage 12 and analysed by immunohistochemistry. Completely ventralized embryos were not analysed. The expected outcome in the case of shuttling is shown in scheme (i), whereas scheme (ii) displays the expected outcome in the absence of shuttling. Owing to the presence of the yolk in the middle of the embryo, we expect to observe the shuttled BMP4–Myc only in the region indicated by the arrow. ar, archenteron; y, yolk; *chd* MO, *chordin* morpholino. **b**–**e**, Shuttling in embryos co-injected with *GFP* and *bmp4myc* mRNA. Stage 12 embryos injected with *bmp4myc* and *GFP* were sectioned along the dorsoventral axis. **b**, Embryo morphology. dm, dorsal mesoderm; yp, yolk-plug; vm, ventral mesoderm. **c**, GFP fluorescence (green) marking the lineage of cells injected with *bmp4myc*. The dorsal mesoderm and dorsal lip are clearly visible (arrowhead). **d**, Distribution of BMP4–Myc. **e**, Merge of **c** and **d**. BMP4–Myc is concentrated at the ventral mesoderm, marked by an arrow, and is absent from the injection site (arrowhead). Auto-fluorescence in the yolk region was detected also in uninjected controls, but was not seen in the mesoderm (not shown). **f**–**i**, Inhibition of shuttling by *chordin* morpholino. Stage 12 embryos injected with *bmp4myc*, *chordin* morpholino and *GFP* were sectioned along the dorsoventral axis. **f**, Embryo morphology. **g**, GFP (green) marking the lineage of the injected cells. The dorsal mesoderm and dorsal lip are clearly visible (arrowhead). **h**, Distribution of BMP4–Myc. **i**, Merge of **g** and **h**. BMP4–Myc is absent from the ventral mesoderm (arrow) but remained at the site of injection (arrowhead). **j**, Statistics. In 50% of embryos injected with *GFP* and *bmp4myc*, BMP4–Myc was separated from the GFP lineage tracer, as predicted by the shuttling model ($n = 36$). Eighty-three per cent of the embryos injected also with *chordin* morpholino showed co-localization of GFP and BMP4–Myc, indicating no shuttling ($n = 42$). $P = 0.001$ (Fisher's exact test).

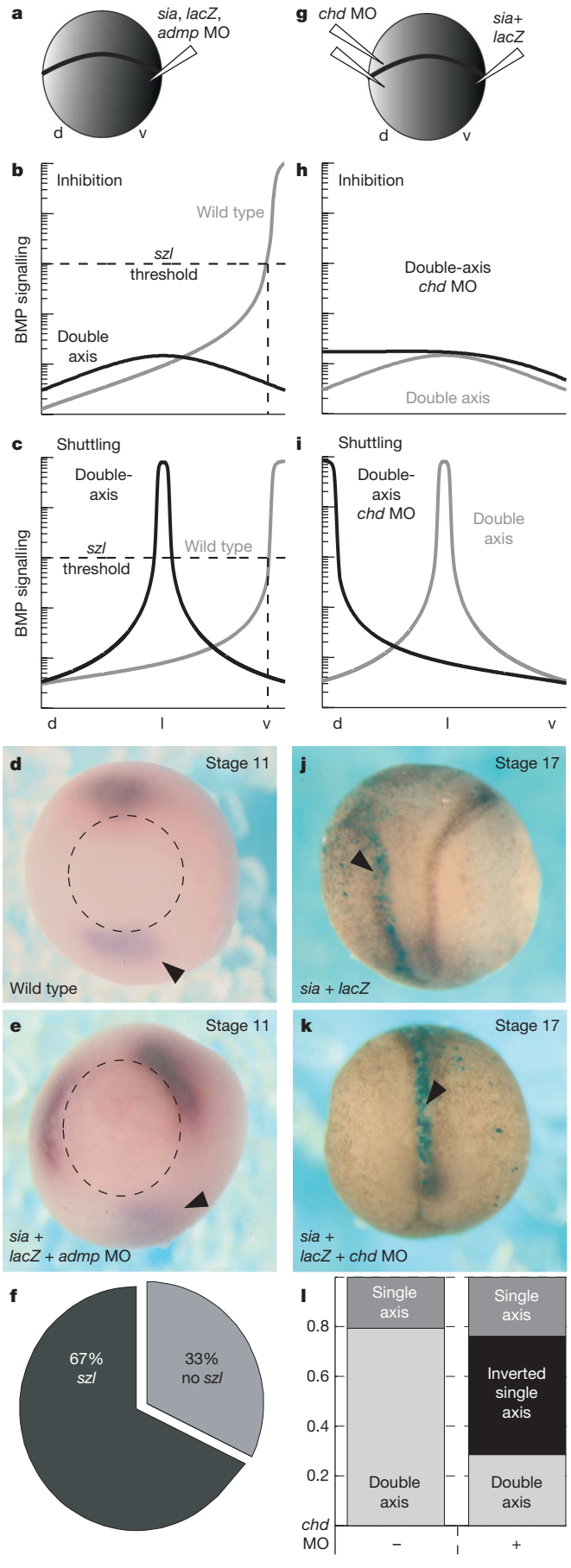

mRNA[41] leads to a secondary axis, with duplicated expression of all dorsal genes[42,43]. We reasoned that the expression domains of the *ventral* genes can provide evidence for shuttling. Consider ventral co-injection of *sia* with *admp* morpholino (Fig. 4a): in such an experiment, the induced organizer serves merely as an additional source of inhibitors. Expression of ventral genes in the region between the two organizers, which corresponds to the lateral region of the wild-type embryo, will occur if the BMP signalling level is increased above its normal level. This will happen only if BMP ligands are concentrated in this region; that is, if the new organizer causes BMP shuttling (Fig. 4b, c). We indeed observed the expression of the ventral marker, *sizzled*, between the two organizers, supporting the shuttling of BMP ligands by components of the new organizer (Fig. 4d–f).

As an additional assay, we attempted to invert the embryonic axis by concomitantly inducing an organizer in the prospective ventral

Figure 4 | Experimental evidence for shuttling in *Xenopus*. **a**–**f**, Expression of ventral genes in double-axis embryos: **a**, Experimental design. Embryos at the two-cell stage were co-injected on the ventral side with *sia* mRNA (27 pg) to induce a secondary organizer, *admp* morpholino (MO; 100 μM) to inhibit the translation of *admp* in the newly induced organizer, and *lacZ* expression plasmid for lineage tracing (see Methods). The injected embryos were grown to stage 11, when expression of *chordin* and *sizzled* was monitored by *in situ* hybridization. **b**, Prediction of inhibition-based model. We solved numerically for the predicted BMP activation profile in double-injected embryos. Because the co-injection of *sia* mRNA and *admp* morpholino culminates in the expression of BMP inhibitors such as Noggin and Chordin (but not BMP ligands) in the induced organizer, the inhibition-based model predicts an overall reduction in the level of BMP activation, and consequently the loss of expression of ventral genes, such as *sizzled*. Grey, wild-type, black-manipulated embryo. d, l, v, dorsal, lateral and ventral, respectively. **c**, Prediction of shuttling-based model. In contrast to the inhibition-based model, this model predicts a re-distribution of BMP, with a significantly elevated level at mid-embryo, allowing the expression of ventral genes. Grey, wild-type, black-manipulated embryo. **d**, Expression of *sizzled* in wild-type embryo. Vegetal view (dorsal to the top) of a stage 11 wild-type embryo stained for *sizzled* (light purple, arrowhead). The dorsal region is marked by *chordin* expression (magenta). Dotted circle marks the blastopore. **e**, Expression of *sizzled* in injected embryo. Embryo orientation as in **d**. β-gal activity was detected in the dorsal–animal part (not shown). *chordin* mRNA is expressed in both organizers, and expression of *sizzled* (arrowhead) is observed between the two sites of *chordin* expression, despite the increased expression of inhibitors. **f**, Fraction of double-injected embryos showing *sizzled* expression as in **e** ($n = 54$). **g**–**l**, Axis inversioning. The experimental design was as follows. Embryos at the two-cell stage were co-injected with *sia* (27 pg) and *lacZ* expression plasmid on the ventral side and *chordin* morpholino (250 μM, double injection) on the dorsal side. The injected embryos were grown to stage 17 and assayed for double-axis formation by morphology. **h**, Prediction of inhibition-based model. We solved numerically for the predicted BMP activation profile in double-injected embryos (Supplementary Information). Within the inhibition-based model, the double-axis observed upon ventral injection of *sia* (grey) is maintained also upon the dorsal co-injection of *chordin* morpholino (black). **i**, Prediction of shuttling-based model. In contrast to the inhibition-based model, the re-distribution of BMP predicted by the shuttling model will lead to a single, inverted axis, with maximal BMP activity at the original dorsal side (black); *sia*-induced double axis in grey. **j**, Double axis in embryo injected with *sia*. Dorsal view of stage 17 embryos; anterior is to the top. Embryos were tested for β-gal expression with X-gal (blue). The induced axis is stained (arrowhead), whereas the original axis is not. **k**, Single inverted axis in embryo co-injected with *sia* and *chordin* morpholino. The single axis expresses β-gal (blue), indicating that it is derived from the induced organizer. Orientation as in **j**. **l**, Fraction of double-injected embryos showing inverted axis. *sia* mRNA induced a secondary axis in 79% of embryos (light grey, $n = 29$). When co-injected with *chordin* morpholino at the dorsal side, a double axis was induced in only 28% of the embryos ($n = 21$). Twenty-four per cent of the embryos had a single axis with no β-gal staining (dark grey), corresponding to embryos where a double axis was not induced (compared with 21% when *sia* was injected without *chordin* morpholino); 48% had a single axis with β-gal staining, corresponding to an axis induced by *sia* mRNA injection (black).

side (through the injection of *sia*) and depleting Chordin from the original organizer (Fig. 4g). Depletion of *chordin* from wild-type embryos has a mild effect, and does not abolish the dorsoventral polarity (probably because of the presence of additional BMP inhibitors at the organizer[15,35], not shown). Accordingly, in the absence of shuttling, the predicted outcome of co-inducing a second organizer while inhibiting Chordin at the original organizer is a double axis, with the original dorsal axis somewhat ventralized (Fig. 4h). In contrast, axis inversion is expected if the induced organizer leads to shuttling of BMP ligands to the original dorsal side, because high BMP signalling will repress the expression of dorsally expressed BMP inhibitors (Fig. 4i). Axis inversion was indeed observed, providing additional support for shuttling (Fig. 4j–l). We note that this experimental outcome is in agreement with the observation that dorsal lip grafts seldom induce secondary axes when prepared from embryos injected with *chordin* morpholino[35], a result that provides additional support for the shuttling mechanism.

Conclusions

We provide a simple, quantitative explanation for the capacity of the *Xenopus* embryo to scale pattern with size. Three key features of the BMP patterning network underlie this capacity. First, patterning is governed by a shuttling-based mechanism, where the BMP ligands are effectively transported by a common BMP inhibitor (Chordin) to the ventral-most part of the embryo, establishing a sharp, power-law decaying activation profile. Second, the presence of two BMP ligands, which differ in their affinity to the inhibitor Chordin, allows for a range of possible steady-state profiles, depending on the relative abundance of the two ligands (Box 1). This is in contrast to the case of a single ligand, where the gradient approaches a unique 'limiting profile' independent of the total ligand level. Finally, the negative auto-repression of the BMP ligand, Admp, is used for sensing embryo size, and effectively tunes the pattern with size. Together, these three features lead to a robust and sharp gradient that is properly scaled with embryo size.

The model we describe is based on what appears to be the core of the patterning network. It can be extended, however, to include additional network components, such as production of Chordin over a large field and the regulation of Chordin expression, xTsg expression[44] and the BMP receptors (Supplementary Information). Further analysis is required to characterize the quantitative contributions of the added network components to patterning, in particular their possible impact on the dynamics of gradient formation.

Our work predicts an evolutionary course that endowed the BMP signalling pathway with two properties that are seemingly mutually exclusive: robust patterning and the ability scale pattern with size. Using the shuttling capacity of the inhibitors with ligands that display similar properties provides robustness but excludes scaling. The evolution of a ligand with unique regulatory properties provides the added feature of scaling, without compromising robustness.

METHODS SUMMARY

Numerical screen. We consider two BMP ligands, [Bmp] and [Admp], an inhibitor, Chordin ([Chd]), the respective complexes [ChdBmp] and [ChdAdmp] and a protease [Xlr]. The model is defined by the following set of reaction diffusion equations:

$$\begin{aligned}
\frac{\partial[\mathrm{Chd}]}{\partial t} &= D_{\mathrm{Chd}}\nabla^2[\mathrm{Chd}] - k_{\mathrm{Admp}}[\mathrm{Admp}][\mathrm{Chd}] - k_{\mathrm{Bmp}}[\mathrm{Bmp}][\mathrm{Chd}] - \lambda_{\mathrm{Chd}}[\mathrm{Xlr}][\mathrm{Chd}] \\
\frac{\partial[\mathrm{Admp}]}{\partial t} &= D_{\mathrm{Lig}}\nabla^2[\mathrm{Admp}] - k_{\mathrm{Admp}}[\mathrm{Admp}][\mathrm{Chd}] + \lambda_{\mathrm{Chd}}^{\mathrm{Admp}}[\mathrm{Xlr}][\mathrm{ChdAdmp}] \\
\frac{\partial[\mathrm{Bmp}]}{\partial t} &= D_{\mathrm{Lig}}\nabla^2[\mathrm{Bmp}] - k_{\mathrm{Bmp}}[\mathrm{Chd}][\mathrm{Bmp}] + \lambda_{\mathrm{Chd}}^{\mathrm{Bmp}}[\mathrm{Xlr}][\mathrm{ChdBmp}] \qquad (3) \\
\frac{\partial[\mathrm{ChdAdmp}]}{\partial t} &= D_{\mathrm{Comp}}\nabla^2[\mathrm{ChdAdmp}] + k_{\mathrm{Admp}}[\mathrm{Admp}][\mathrm{Chd}] - \lambda_{\mathrm{Chd}}^{\mathrm{Admp}}[\mathrm{Xlr}][\mathrm{ChdAdmp}] \\
\frac{\partial[\mathrm{ChdBmp}]}{\partial t} &= D_{\mathrm{Comp}}\nabla^2[\mathrm{ChdBmp}] + k_{\mathrm{Bmp}}[\mathrm{Bmp}][\mathrm{Chd}] - \lambda_{\mathrm{Chd}}^{\mathrm{Bmp}}[\mathrm{Xlr}][\mathrm{ChdBmp}]
\end{aligned}$$

The steady-state signalling profile $S(x) = [\mathrm{Admp}](x) + [\mathrm{Bmp}](x)$ is considered as the biologically relevant output.

Boundary conditions. All fluxes vanish at $x = 0$ and $x = L$ except a constant flux of Chordin, and signal-dependent flux of Admp at the dorsal pole ($x = L$).

Screen parameters. The following nine parameters were changed in the screen: diffusion coefficients, binding of Chordin with Bmp or Admp, cleavage of Chordin by Xlr when it is free or in complex with Bmp or Admp, and the Chordin flux. The respective parameter space was scanned systematically with each parameter modified by at least two orders of magnitude, and the model was solved numerically for over 26,000 parameter sets. A network was marked 'consistent' if the associated signalling profile displayed proper dorsoventral polarity, scaled with embryo size, and was robust to parameter variations (Supplementary Information).

The shuttling coefficient S_h measures the dynamic range of the total ligand, normalized by the dynamic range of the total free ligand. For ideal shuttling $S_h \approx 1$, whereas for the inhibitory model $S_h \approx 0$.

Embryo manipulation. Embryos at the desired stage were fixed in MEMFA and processed for *in situ* hybridization. Antisense morpholino oligonucleotides and mRNA were injected to embryos at the two-cell stage. β-Galactosidase (β-gal) and *GFP*[45] activities were used for lineage tracing. Embryos were injected in $1 \times$ MBSH, and raised to the desired stage in $0.1 \times$ MBSH.

Immunohistochemistry. Embryos were fixed, re-hydrated and bisected along the dorsoventral axis. After blocking, embryos were incubated with primary antibody overnight, and then labelled with a fluorescent secondary antibody.

Full Methods and any associated references are available in the online version of the paper at www.nature.com/nature.

Received 27 January; accepted 8 May 2008.

1. Waddington, C. H. Canalization of development and the inheritance of acquired characters. *Nature* **150,** 563–565 (1942).
2. Kirschner, M. & Gerhart, J. Evolvability. *Proc. Natl Acad. Sci. USA* **95,** 8420–8427 (1998).
3. De Robertis, E. M. Spemann's organizer and self-regulation in amphibian embryos. *Nature Rev. Mol. Cell Biol.* **7,** 296–302 (2006).
4. Spemann, H. *Embryonic Development and Induction* (Yale Univ. Press, New Haven, 1938).
5. Spemann, H. & Mangold, H. Induction of embryonic primordia by implantation of organizers from a different species. *Roux's Arch. Entw. Mech.* **100,** 599–638 (1924).
6. Harland, R. M. Neural induction in *Xenopus*. *Curr. Opin. Genet. Dev.* **4,** 543–549 (1994).
7. Cooke, J. Scale of body pattern adjusts to available cell number in amphibian embryos. *Nature* **290,** 775–778 (1981).
8. Lowe, C. J. *et al.* Dorsoventral patterning in hemichordates: insights into early chordate evolution. *PLoS Biol.* **4,** e291 (2006).
9. Marques, G. *et al.* Production of a DPP activity gradient in the early *Drosophila* embryo through the opposing actions of the SOG and TLD proteins. *Cell* **91,** 417–426 (1997).
10. Ferguson, E. L. Conservation of dorsal–ventral patterning in arthropods and chordates. *Curr. Opin. Genet. Dev.* **6,** 424–431 (1996).
11. De Robertis, E. M. & Kuroda, H. Dorsal-ventral patterning and neural induction in *Xenopus* embryos. *Annu. Rev. Cell Dev. Biol.* **20,** 285–308 (2004).
12. Francois, V. & Bier, E. *Xenopus* chordin and *Drosophila* short gastrulation genes encode homologous proteins functioning in dorsal–ventral axis formation. *Cell* **80,** 19–20 (1995).
13. Sasai, Y. *et al. Xenopus* chordin: a novel dorsalizing factor activated by organizer-specific homeobox genes. *Cell* **79,** 779–790 (1994).
14. Sasai, Y., Lu, B., Steinbeisser, H. & De Robertis, E. M. Regulation of neural induction by the Chd and Bmp-4 antagonistic patterning signals in *Xenopus*. *Nature* **376,** 333–336 (1995).
15. Khokha, M. K., Yeh, J., Grammer, T. C. & Harland, R. M. Depletion of three BMP antagonists from Spemann's organizer leads to a catastrophic loss of dorsal structures. *Dev. Cell* **8,** 401–411 (2005).
16. Ross, J. J. *et al.* Twisted gastrulation is a conserved extracellular BMP antagonist. *Nature* **410,** 479–483 (2001).
17. Oelgeschlager, M., Larrain, J., Geissert, D. & De Robertis, E. M. The evolutionarily conserved BMP-binding protein Twisted gastrulation promotes BMP signalling. *Nature* **405,** 757–763 (2000).
18. Chang, C. *et al.* Twisted gastrulation can function as a BMP antagonist. *Nature* **410,** 483–487 (2001).
19. Larrain, J. *et al.* Proteolytic cleavage of Chordin as a switch for the dual activities of Twisted gastrulation in BMP signaling. *Development* **128,** 4439–4447 (2001).
20. Goodman, S. A. *et al.* BMP1-related metalloproteinases promote the development of ventral mesoderm in early *Xenopus* embryos. *Dev. Biol.* **195,** 144–157 (1998).
21. Piccolo, S. *et al.* Cleavage of Chordin by Xolloid metalloprotease suggests a role for proteolytic processing in the regulation of Spemann organizer activity. *Cell* **91,** 407–416 (1997).
22. Dosch, R. & Niehrs, C. Requirement for anti-dorsalizing morphogenetic protein in organizer patterning. *Mech. Dev.* **90,** 195–203 (2000).

23. Moos, M. Jr, Wang, S. & Krinks, M. Anti-dorsalizing morphogenetic protein is a novel TGF-beta homolog expressed in the Spemann organizer. *Development* **121,** 4293–4301 (1995).
24. Reversade, B. & De Robertis, E. M. Regulation of ADMP and BMP2/4/7 at opposite embryonic poles generates a self-regulating morphogenetic field. *Cell* **123,** 1147–1160 (2005).
25. Decotto, E. & Ferguson, E. L. A positive role for Short gastrulation in modulating BMP signaling during dorsoventral patterning in the *Drosophila* embryo. *Development* **128,** 3831–3841 (2001).
26. Eldar, A. *et al.* Robustness of the BMP morphogen gradient in *Drosophila* embryonic patterning. *Nature* **419,** 304–308 (2002).
27. Umulis, D. M., Serpe, M., O'Connor, M. B. & Othmer, H. G. Robust, bistable patterning of the dorsal surface of the *Drosophila* embryo. *Proc. Natl Acad. Sci. USA* **103,** 11613–11618 (2006).
28. Mizutani, C. M. *et al.* Formation of the BMP activity gradient in the *Drosophila* embryo. *Dev. Cell* **8,** 915–924 (2005).
29. Meinhardt, H. & Roth, S. Developmental biology: sharp peaks from shallow sources. *Nature* **419,** 261–262 (2002).
30. Shimmi, O., Umulis, D., Othmer, H. & O'Connor, M. B. Facilitated transport of a Dpp/Scw heterodimer by Sog/Tsg leads to robust patterning of the *Drosophila* blastoderm embryo. *Cell* **120,** 873–886 (2005).
31. Wang, Y. C. & Ferguson, E. L. Spatial bistability of Dpp-receptor interactions during *Drosophila* dorsal–ventral patterning. *Nature* **434,** 229–234 (2005).
32. van der Zee, M., Stockhammer, O., von Levetzow, C., da Fonseca, R. N. & Roth, S. Sog/Chordin is required for ventral-to-dorsal Dpp/BMP transport and head formation in a short germ insect. *Proc. Natl Acad. Sci. USA* **103,** 16307–16312 (2006).
33. O'Connor, M. B., Umulis, D., Othmer, H. G. & Blair, S. S. Shaping BMP morphogen gradients in the *Drosophila* embryo and pupal wing. *Development* **133,** 183–193 (2006).
34. Eldar, A., Shilo, B. Z. & Barkai, N. Elucidating mechanisms underlying robustness of morphogen gradients. *Curr. Opin. Genet. Dev.* **14,** 435–439 (2004).
35. Oelgeschlager, M., Kuroda, H., Reversade, B. & De Robertis, E. M. Chordin is required for the Spemann organizer transplantation phenomenon in *Xenopus* embryos. *Dev. Cell* **4,** 219–230 (2003).
36. Reversade, B., Kuroda, H., Lee, H., Mays, A. & De Robertis, E. M. Depletion of Bmp2, Bmp4, Bmp7 and Spemann organizer signals induces massive brain formation in *Xenopus* embryos. *Development* **132,** 3381–3392 (2005).
37. Ohkawara, B., Iemura, S.-I., ten Dijke, P. & Ueno, N. Action range of BMP is defined by its N-terminal basic amino acid core. *Curr. Biol.* **12,** 205–209 (2002).
38. Lander, A. D., Nie, Q. & Wan, F. Y. Do morphogen gradients arise by diffusion? *Dev. Cell* **2,** 785–796 (2002).
39. Lee, H. X., Ambrosio, A. L., Reversade, B. & De Robertis, E. M. Embryonic dorsal–ventral signaling: secreted frizzled-related proteins as inhibitors of tolloid proteinases. *Cell* **124,** 147–159 (2006).
40. Jones, C. M., Armes, N. & Smith, J. C. Signalling by TGF-β family members: short-range effects of Xnr-2 and BMP-4 contrast with the long-range effects of activin. *Curr. Biol.* **6,** 1468–1475 (1996).
41. Lemaire, P., Garrett, N. & Gurdon, J. B. Expression cloning of *Siamois*, a *Xenopus* homeobox gene expressed in dorsal–vegetal cells of blastulae and able to induce a complete secondary axis. *Cell* **81,** 85–94 (1995).
42. Marom, K., Levy, V., Pillemer, G. & Fainsod, A. Temporal analysis of the early BMP functions identifies distinct anti-organizer and mesoderm patterning phases. *Dev. Biol.* **282,** 442–454 (2005).
43. Fagotto, F., Guger, K. & Gumbiner, B. Induction of the primary dorsalizing center in *Xenopus* by the Wnt/GSK/beta-catenin signaling pathway, but not by Vg1, Activin or Noggin. *Development* **124,** 453–460 (1997).
44. Collavin, L. & Kirschner, M. W. The secreted Frizzled-related protein Sizzled functions as a negative feedback regulator of extreme ventral mesoderm. *Development* **130,** 805–816 (2003).
45. Zernicka-Goetz, M. *et al.* An indelible lineage marker for *Xenopus* using a mutated green fluorescent protein. *Development* **122,** 3719–3724 (1996).

Supplementary Information is linked to the online version of the paper at www.nature.com/nature.

Acknowledgements We thank J. Christian for the BMP4 constructs, and the members of our groups for discussions and help with the experiments. This work was supported by Minerva, the Israel Science Foundation and the Hellen and Martin Kimmel award for innovative investigations to N.B. and a grant from the Israel Science Foundation and the Wolfson Family Chair in Genetics to A.F. B-Z.S. holds the Hilda and Cecil Lewis Professorial chair in Molecular Genetics.

Author Information Reprints and permissions information is available at www.nature.com/reprints. Correspondence and requests for materials should be addressed to N.B. (Naama.barkai@weizmann.ac.il) or A.F. (fainsod@cc.huji.ac.il).

METHODS

Numerical screen. Full details of the numerical screen are provided in the Supplementary Information (Section 1). Here we summarize the basic methods. Our model does not consider the mechanism underlying the formation of the organizer, but only the subsequent steps[46]. We consider two BMP ligands, [Bmp] and [Admp], an inhibitor, Chordin ([Chd]), the respective complexes [ChdBmp] and [ChdAdmp] and a protease [Xlr]. The model is defined by the following set of reaction diffusion equations:

$$\begin{aligned}
\frac{\partial[\mathrm{Chd}]}{\partial t} &= D_{\mathrm{Chd}}\nabla^2[\mathrm{Chd}] - k_{\mathrm{Admp}}[\mathrm{Admp}][\mathrm{Chd}] - k_{\mathrm{Bmp}}[\mathrm{Bmp}][\mathrm{Chd}] - \lambda_{\mathrm{Chd}}[\mathrm{Xlr}][\mathrm{Chd}] \\
\frac{\partial[\mathrm{Admp}]}{\partial t} &= D_{\mathrm{Lig}}\nabla^2[\mathrm{Admp}] - k_{\mathrm{Admp}}[\mathrm{Admp}][\mathrm{Chd}] + \lambda_{\mathrm{Chd}}^{\mathrm{Admp}}[\mathrm{Xlr}][\mathrm{ChdAdmp}] \\
\frac{\partial[\mathrm{Bmp}]}{\partial t} &= D_{\mathrm{Lig}}\nabla^2[\mathrm{Bmp}] - k_{\mathrm{Bmp}}[\mathrm{Chd}][\mathrm{Bmp}] + \lambda_{\mathrm{Chd}}^{\mathrm{Bmp}}[\mathrm{Xlr}][\mathrm{ChdBmp}] \qquad (3) \\
\frac{\partial[\mathrm{ChdAdmp}]}{\partial t} &= D_{\mathrm{Comp}}\nabla^2[\mathrm{ChdAdmp}] + k_{\mathrm{Admp}}[\mathrm{Admp}][\mathrm{Chd}] - \lambda_{\mathrm{Chd}}^{\mathrm{Admp}}[\mathrm{Xlr}][\mathrm{ChdAdmp}] \\
\frac{\partial[\mathrm{ChdBmp}]}{\partial t} &= D_{\mathrm{Comp}}\nabla^2[\mathrm{ChdBmp}] + k_{\mathrm{Bmp}}[\mathrm{Bmp}][\mathrm{Chd}] - \lambda_{\mathrm{Chd}}^{\mathrm{Bmp}}[\mathrm{Xlr}][\mathrm{ChdBmp}]
\end{aligned}$$

The steady-state signalling profile $S(x) = [Admp](x) + [Bmp](x)$ is considered as the biologically relevant output.

Boundary conditions. All fluxes vanish at $x = 0$ and $x = L$ except a constant flux of Chordin, η_{Chd}, and signal-dependent flux of Admp, $\alpha(S)$, at the dorsal pole ($x = L$), with $\alpha(S) = 10^{-3}\dfrac{T_{\mathrm{Admp}}^4}{T_{\mathrm{Admp}}^4 + S(L)^4}\,\mu\mathrm{M}\mu\mathrm{m}\mathrm{s}^{-1}$.

Screen parameters. The following parameters were changed in the screen: diffusion coefficients of Chordin, the ligands and the Chordin–ligand complexes (D_{Chd}, D_{Lig}, D_{Comp}), binding of the Chordin with Bmp or Admp (k_{Bmp}, k_{Admp}), cleavage of the Chordin by Xlr when it is free or in complex with Bmp or Admp $\left(\lambda_{\mathrm{Chd}}, \lambda_{\mathrm{Chd}}^{\mathrm{Bmp}}, \lambda_{\mathrm{Chd}}^{\mathrm{Admp}}\right)$ and the Chordin flux (η_{Chd}). The respective nine-dimensional parameters space was scanned systematically with each parameter modified by at least two orders of magnitude. Log mid-values of the parameters were: $D_{\mathrm{Chd}} = D_{\mathrm{Lig}} = D_{\mathrm{Comp}} = 1\,\mu\mathrm{m}^2\,\mathrm{s}^{-1}$, $k_{\mathrm{Bmp}} = k_{\mathrm{Admp}} = 0.1\,\mu\mathrm{M}^{-1}\,\mathrm{s}^{-1}$, $\lambda_{\mathrm{Chd}} = \lambda_{\mathrm{Chd}}^{\mathrm{Bmp}} = \lambda_{\mathrm{Chd}}^{\mathrm{Admp}} = 0.1\mu\mathrm{M}^{-1}\mathrm{s}^{-1}$, $\eta_{\mathrm{Chd}} = 10^{1.5}\,\mu\mathrm{M}\,\mu\mathrm{m}\,\mathrm{s}^{-1}$. Xlr concentration was set to [Xlr] = 0.01 μM and whole embryo length $L = 1{,}000\,\mu\mathrm{m}$.

Screen execution. The model was solved numerically for over 26,000 sets of parameters. A network was marked 'consistent' if the associated signalling profile displayed proper dorsoventral polarity, scaled with embryo size and was robust to parameter variations (see Supplementary Information for precise definitions).

Shuttling coefficient. The shuttling coefficient S_{h} measures to the dynamic range of the total ligand $S^{\mathrm{tot}}(x) = S(x) + [\mathrm{ChdAdmp}](x) + [\mathrm{ChdBmp}](x)$, normalized by the dynamic range of the total free ligand, $S(x) = [\mathrm{Admp}](x) + [\mathrm{Bmp}](x)$.

$S_h = \dfrac{\delta S^{\mathrm{tot}}}{\delta S}$, where $\delta S = \dfrac{\max(S) - \min(S)}{\max(S)}$; max(S) and min(S) refer to the maximal and minimal levels of $S(x)$ over the entire embryo, respectively. δS^{tot} is defined similarly. For ideal shuttling $S_{\mathrm{h}} \approx 1$, whereas for the inhibitory model $S_{\mathrm{h}} \approx 0$.

Embryo manipulation. *Xenopus laevis* were purchased from Xenopus1. Embryos were obtained by *in vitro* fertilization and incubated in 0.1 × modified Barth's solution (MBSH). Dorsal-half embryos: stage 8.5 embryos were dechorionated in 0.3 ×MBSH and cut into a dorsal and ventral halves. Dorsal-half embryos were cultured in fresh 0.3 × MBSH until the desired stage.

***In situ* hybridization and probes.** Embryos at the desired stage were fixed in MEMFA and processed for *in situ* hybridization, as described[47]. Digoxigenin (Dig)-labelled RNA and fluorescein probes were transcribed *in vitro* using the RiboMax kit (Promega), and the Dig. RNA labelling mix (Roche) or Fluorescein RNA labelling mix (Roche), respectively. The probes used in the *in situ* hybridization procedure were *chordin*, the Δ59 clone[13] and *sizzled*[48].

Morpholino oligonucleotides, mRNA injections and lineage tracing. Antisense morpholino oligonucleotides (morpholino) were obtained from Gene Tools LLC for *Xenopus laevis. admp* morpholino[24] and *chordin* morpholino (both pseudoalleles[35]) were injected into embryos at the two-cell stage as described in the text. mRNA for microinjection was prepared using the RiboMax kit (Promega), and adding cap analogue (Roche, Pharmacia) at a ratio of 1:5 (GTP:cap analogue). *sia*[41] mRNA was injected ventrally at the two-cell stage. *GFP*[45] and *bmp4myc*[49] were injected dorsally at the two-cell stage as described in the text. β-Gal activity was used for lineage tracing: a *lacZ* expression plasmid (CMV–LacZ), was injected at 30 ng $\mu\mathrm{l}^{-1}$ as described in the text. Staining of the β-gal activity was done as described[42]. Embryos were injected in 1 × MBSH buffer, and raised to the desired stage in 0.1 × MBSH buffer.

Immunohistochemistry. Embryos were fixed in MEMFA for 1 h and stored in Dent's solution (20% dimethylsulphoxide in methanol) at −20 °C overnight. Rehydrated embryos were bisected along the dorsoventral axis, and blocked in PBT (PBS, 2 mg ml^{-1} BSA, 0.1% Triton X-100) plus 10% normal bovine serum. Embryos were incubated with primary antibody (anti-Myc 9E10, 1:100, 4 °C, overnight). The embryos were then washed five times in PBT and incubated with a cy3 fluorescent-labelled secondary antibody (1:500, 4 °C, overnight).

46. Meinhardt, H. Primary body axes of vertebrates: generation of a near-cartesian coordinate system and the role of Spemann-type organizer. *Dev. Dyn.* **235**, 2907–2919 (2006).
47. Fainsod, A., Steinbeisser, H. & De Robertis, E. M. On the function of BMP-4 in patterning the marginal zone of the *Xenopus* embryo. *EMBO J.* **13**, 5015–5025 (1994).
48. Salic, A. N., Kroll, K. L., Evans, L. M. & Kirschner, M. W. Sizzled: a secreted Xwnt8 antagonist expressed in the ventral marginal zone of *Xenopus* embryos. *Development* **124**, 4739–4748 (1997).
49. Sopory, S., Nelsen, S. M., Degnin, C., Wong, C. & Christian, J. L. Regulation of bone morphogenetic protein-4 activity by sequence elements within the prodomain. *J. Biol. Chem.* **281**, 34021–34031 (2006).